Characterization of Adaptation Motors in Saccular Hair Cells by Fluctuation Analysis

Jonathan E. Frank,* Vladislav Markin,† and Fernán Jaramillo*
*Department of Biology, Carleton College, Northfield, Minnesota 55057, and †Department of Anesthesiology, University of Texas Southwestern Medical Center, Dallas, Texas 75235 USA

ABSTRACT The mechanical sensitivity of hair cells, the sensory receptors of the vestibular and auditory systems, is maintained by adaptation, which resets the transducer to cancel the effects of static stimuli. Adaptation motors in hair cells can be experimentally activated by externally applying a transduction channel blocker to the hair bundle, causing the hair bundle to move in the negative direction. We studied the variance in the position of the hair bundle during these displacements and found that it increases as the bundle moves to its new position. Often the variance peaks, and then declines to a steady-state value. We describe both displacement and variance with a model in which a motor acting on the bundle takes ~3.6-nm steps whose frequency (~22 s^{-1}) declines with the motor's load.

INTRODUCTION

Hair cells, the sensory receptors of the vestibular and auditory systems, are graced with a hair bundle, an organelle of exquisite mechanical sensitivity. The design of the hair bundle poses a challenge, i.e., how to maintain its sensitivity to small deflections in the presence of large steady offsets in the bundle's position, which can be caused by static stimuli such as postural changes. The solution to this problem is adaptation, which in the hair cell resets the transducer to cancel the effects of static stimuli.

Adaptation is the result of at least two processes that differ in their time constants by over an order of magnitude (for reviews on both types of adaptation see Eatock, 2000; Holt and Corey, 2000). The fast component ($\tau \sim 1$ ms), which is best understood in turtle auditory hair cells, can be explained by a model in which Ca^{2+}, entering through a transduction channel, binds to an intracellular site, resulting in a change in the probability of the channel being open (Ricci et al., 1998; Wu et al. 1999). The slow adaptation component (τ of a few tens of milliseconds, depending on the cell) has been linked to the activity of myosin motors (Gillespie and Corey, 1997; see model in Fig. 1).

Adaptation motors regulate tension in the tip links, which are thought to gate the mechanoelectrical transduction channels. Therefore, one can infer motor activity from the time course of transduction currents. Alternatively, one can measure the mechanical forces that motors exert, providing insight into aspects of motor function that cannot be approached electrophysiologically. Here we take advantage of the open channel blocker gentamicin to prevent the influx of Ca^{2+} through transduction channels that are open at rest, thus activating the adaptation motors. In the presence of high concentration of gentamicin, a channel that opens is rapidly blocked. Thus, within a few milliseconds, nearly all transduction channels are trapped in the blocked state (Jaramillo and Hudspeth, 1993). The intracellular reduction in the concentration of Ca^{2+} near the channel, which is probably sensed by calmodulin, results in an increase in motor activity that causes the motors to climb, increasing the tension in the tip links, and causing the hair bundle to undergo a slight movement in the negative direction (toward the shorter stereocilia).

It is believed that every tip link is coupled to a motor complex, which, in turn, is thought to comprise at least several dozen myosin molecules. In mice vestibular hair cells, this motor role is currently attributed to Myo1c (Holt et al., 2002). However, Myo7a has been implicated in adaptation in mouse cochlear hair cells, although its function there might be more complex, involving not only a motor activity but a membrane-to-cytoskeleton anchoring role (Kros et al., 2002). Because the mechanical cycle of the myosins is a stochastic process, we anticipated that their activity would cause random fluctuations in the position of the hair bundle. Furthermore, one would expect that an increase in motor activity would cause an increase of such fluctuations. To test this idea, we subjected hair bundles to multiple presentations of gentamicin, and measured not only the bundle's displacement, but the displacement's variance as a function of time. The results presented here, which confirm our prediction, are consistent with a simple model of motor function.

MATERIALS AND METHODS

Preparation

Experiments were performed in the isolated saccular macula of bullfrogs (*Rana catesbeiana*), using techniques described previously (Howard and Hudspeth, 1988; Jaramillo and Hudspeth, 1993). The saccular macula was isolated, and digested for 10 min with 75 μg/ml protease XXIV (Sigma, St. Louis, MO) at room temperature (20–25°C) in a perilymph-like saline ((mM) 110 NaCl, 2 KCl, 0.1 $CaCl_2$, 3 glucose, 5 HEPES, pH 7.25 with 1N

Submitted July 1, 2002 and accepted for publication August 9, 2002.

Address reprint requests to Fernán Jaramillo, Dept. of Biology, Carleton College, Northfield, MN 55057-4025. Tel.: 507-646-4392; Fax: 507-646-5757; E-mail: fjaramil@carleton.edu.

0006-3495/02/12/3188/14 $2.00

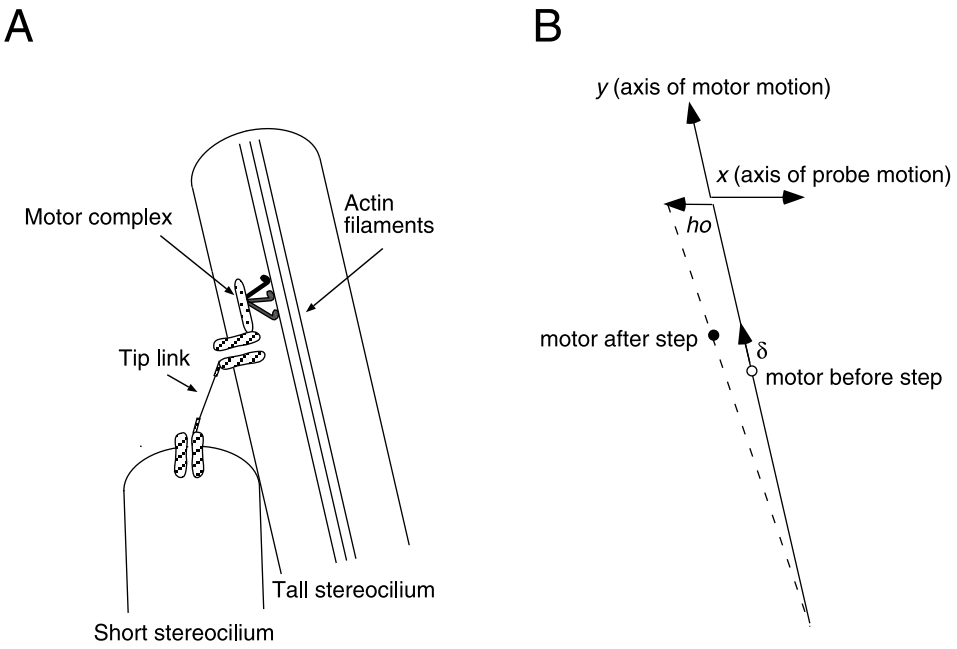

FIGURE 1 Slow adaptation in hair cells. A hypothetical mechanism of slow adaptation, which, in the *Rana catesbeiana* hair cell, resets the transduction apparatus within a few tens of milliseconds following a stimulus. (*A*) The hair bundle's stereocilia are joined near their tips by tip links (only two stereocilia shown), which are thought to regulate the gating of transduction ion. The top transduction channel is coupled to a cytoskeletal complex containing a multimolecular motor, which is thought to be composed of about 100 myosin molecules (three are shown for illustration, molecules not drawn to scale). The activity of these myosins is regulated, via calmodulin, by the intracellular concentration of Ca^{2+}. (*B*) The increase in tension of the tip link, which results from a myosin's climbing step, δ, pushes the hair bundle and the attached probe in the negative direction (toward the left in the figure) a distance h_0. The *y* and *x* axes, which are not orthogonal, represent the axis along which the motor complex moves, and the bundle's axis of mechanoelectrical sensitivity, respectively.

NaOH). After digestion, the macula was washed twice in fresh saline (minus the protease), attached to the glass bottom of a recording chamber using biological glue (Cell-Tak, BD Biosciences, Bedford, MA), and the otholitic membrane carefully removed using fine forceps. The chamber was then transferred to a fixed, rigid stage (Meridian Manufacturing Inc., Kent, WA) for recording. An upright microscope (Nikon, E600 FN), mounted on a translation stage, was used to observe the preparation. Imaging was performed under Nomarski optics, using a 60×, water immersion objective (numerical aperture 1.0). Recordings were performed in the perilymph-like saline described above. For control experiments (see Fig. 4) the saline was supplemented with either 100 μM gentamicin sulfate, or 5 mM BAPTA (1,2-bis(o-aminophenoxy)ethane-*N*,*N*,*N*′,*N*′-tetraacetic acid).

Photodiode detector

To monitor the position of the translucent hair bundles, a gold-coated flexible glass probe was attached to the bundle's kinociliary bulb. Care was exerted to prevent biasing the bundle when the probe was attached. However, the absolute position of the bundle at the time of contact was not determined. Probes (0.5–1.0 μm in diameter at their tip) were manufactured from 1 mm borosilicate stock using a horizontal electrode puller (P-80 PC, Sutter, Novato, CA), and trimmed with iridectomy scissors to attain a stiffness at the tip comparable to that of a hair bundle (~1 mN m^{-1}, range 0.39–1.1 mN m^{-1}). The image of the probe's distal end was magnified 1000× and projected onto a dual photodiode (EG-G Optoelectronics, Vaudreuil, QC, Canada), and the photocurrents converted to voltages by current-to-voltage converters with an effective bandwidth of 5.3 kHz. The photocurrents difference was amplified, low pass filtered at 1.0 kHz (four-pole Bessel), and sampled at 2.5 kHz by a computer using a 12 bit data-acquisition board (National Instruments, E-series) using LabView. The stiffness of the flexible probe was estimated from the probe's variance of motion, which, in turn, was estimated from the photodiode's output (Howard and Hudspeth, 1988). Positioning of the probe's image with respect to the photodiode was accomplished by projecting the phototube's image onto a small screen. Immediately before iontophoretic stimulation, the photodiode was automatically centered on the flexible fiber and a series of 5-μm displacements imparted on the photodiode for calibration purposes.

To reduce mechanical noise, the microscope was placed on a vibration isolation table (Technical Manufacturing), standing on a 12 × 12-foot concrete platform separated by a 1-inch gap on its sides from the building's concrete floor. Fig. 2, obtained by monitoring fluctuations of a stiff probe, gives an indication of the residual, uncontrolled mechanical vibrations. In general, residual mechanical noise was ~1 nm (root mean square) in the 1.0-kHz bandwidth.

Iontophoresis

Iontophoretic electrodes were used to apply gentamicin to the hair bundle as described previously (Jaramillo and Hudspeth, 1991, 1993). Although other transduction channel blockers such as amiloride, La^{3+}, etc., can be applied iontophoretically, their relatively high mobility, lack of solubility, and relatively low affinity for the channel would require enormous currents to produce an effective blocking concentration. Although adaptation motors can also be activated by lowering extracellular Ca^{2+} with chelators such as BAPTA, these also cause tip links to break (Assad et al., 1991; Jaramillo and Hudspeth, 1993). Thus, aminoglycosides such as gentamicin

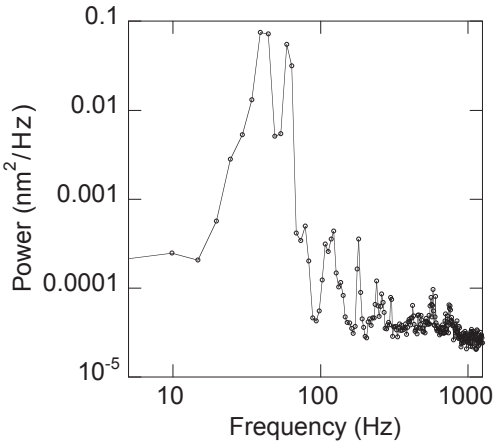

FIGURE 2 Power spectrum of fluctuations observed for a stiff glass probe. Noise around 40 Hz could not be entirely removed. The root mean square of motion for this probe was 1.0 nm. This gives an indication of residual uncontrolled mechanical noise in our setup.

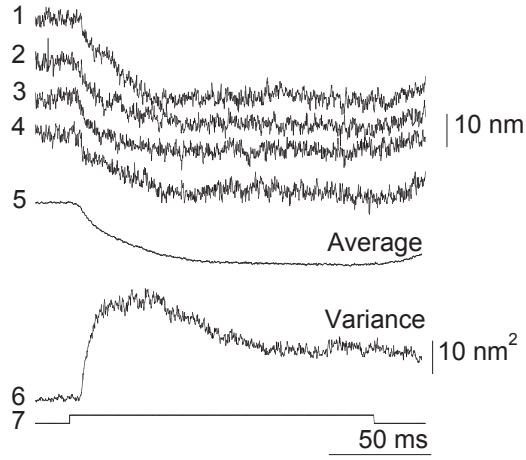

FIGURE 3 Hair bundle responses to gentamicin. The cell was subjected to 80-nA, 150-ms applications of gentamicin (*trace 7*). After the pulse, the bundle moved in the negative direction (*sample traces 1–4*). Responses were averaged (*trace 5*) and the variance (*trace 6*) computed by subtracting the mean from each one of the 82 displacement traces and averaging the squared differences.

provide the best means to rapidly block transduction channels with minimal mechanical disturbance. Conventional capillary-filled glass microelectrodes were filled with a 500-mM aqueous solution of gentamicin sulfate (Sigma). This solution was supplemented with 20 mM KCl to prevent the polarization of the AgCl electrode. The electrode filling solution had a slightly acidic pH, which ensures that the drug's amino groups are protonated. Iontophoretic electrodes, when filled with the aminoglycoside solution, had resistances of ~300 MΩ.

In general, ~50 iontophoretic pulses (150 ms each) were applied to a given cell at a frequency of ~2 Hz. The frequency of stimulation was adjusted from cell to cell to ensure that the bundle had returned to its original position before administering a new pulse. Occasionally, a pulse series had to be interrupted if it appeared that the cell was fatiguing, or when the iontophoretic electrode became blocked. However, in most cases, there was no apparent decline in a cell's responses during a stimulus series. Iontophoretic currents (0–100 nA, −2 nA retaining current) were delivered using an Ion-100 iontophoretic generator with ±130-V compliance (Dagan Corporation, Minneapolis, MN). Negative current pulses were applied as a control. Negative iontophoretic pulses often produced a small probe motion in the positive direction. This motion, whose amplitude was less than 10% of the response to positive pulses, was an artifact that could be elicited in the absence of a bundle. Similarly, very large positive pulses ($I > 100$ nA), delivered with KCl-filled electrodes, caused a small motion in the negative direction. Therefore, these large amplitudes were not used in our experiments. When a cell gave unusually good responses, we carefully moved the cell away, leaving the probe and iontophoretic electrode in place. The data was accepted if the observed artifact was less than 10% of the response obtained with the hair cell. In many cases, we obtained responses without artifact (see also Fig. 4).

We estimate the concentration (C) of gentamicin at a distance (r) from the tip of the iontophoretic electrode according to $C(t) = (\zeta i/4\pi FDr)\mathrm{erfc}(r/\sqrt{4Dt})$ (Berg, 1983). Here ζ is an estimate of the ratio of gentamicin's transference number to its valence (0.03) obtained for similar microelectrodes (Jaramillo and Hudspeth, 1991), i is the iontophoretic current, F is Faraday's constant, D is gentamicin's estimated diffusion coefficient ($\sim 4.0\ 10^{-10}\ \mathrm{m^2\ s^{-1}}$, (Jaramillo and Hudspeth, 1991)), and erfc represents the complementary error function. We estimate that, within a span of 10 ms, the concentration of gentamicin at a distance of 5 μm from the electrode rises from negligible values to 70 μM, a value sufficient to block 90% of the transduction channels, given gentamicin's Kd for channel blocking of 8 μM (Kroese et al., 1989). By the end of the pulse, the concentration of gentamicin should be near 400 μM. These values are about one order of magnitude lower than those calculated by others, but the values obtained by these authors rely on a relatively high estimate of gentamicin's diffusion coefficient and a high estimate (rather than an experimental determination) of the aminoglycoside's transference number (Denk et al., 1992).

Data analysis

Displacement traces were inspected individually. A few traces in every run were discarded if they seemed to be corrupted by artifactual motions due to uncontrolled mechanical noise. Such artifacts were elicited by occasional disturbances in the recording room: door slamming in the building, building equipment coming on, etc. Traces were averaged, and the variance computed by subtracting the mean from every accepted trace, and averaging the squared differences. Data are presented as mean ± SD.

RESULTS

Response to gentamicin

We measured the response of hair cells to iontophoretic applications of gentamicin. Hair bundles (96 out of 124 tested) moved in the negative direction, with a nearly exponential time course, after the onset of the iontophoretic pulse (Fig. 3). We assume that cells that failed to respond to gentamicin had a damaged transduction apparatus, which is relatively common after dissection and enzymatic digestion (also see Specificity of Gentamicin Action below). Bundle motion followed the pulse with a delay of a few milliseconds, consistent with the time required for diffusion of gentamicin from the electrode's tip to the transduction channels. This delay is longer than seen previously (Jaramillo and Hudspeth, 1993) because, to avoid iontophoretic artifacts, the tip of the iontophoretic electrode was placed at least 5 μm away from the bundle. This increased distance

tends to produce a more graded increase in blocker concentration, instead of a step, therefore distorting (in effect smoothing out) the fast mechanical transient due to channel block (Jaramillo and Hudspeth, 1993). This effect, which consists of a small decrease in the tip link tension as channels open (a channel must open before it is blocked) produces a minor deflection of the bundle in the positive direction. This component of motion was not considered further (see Transduction Channel Gating Effects in the Discussion).

Specificity of gentamicin action

A significant fraction of the cells (28/124) failed to respond to gentamicin, an observation consistent with the fact that some hair cells undergo hair-bundle damage during enzymatic digestion and peeling of the otholitic membrane. In the majority of these cells, there was no discernable motion associated with iontophoresis, indicating that responses depend on the specific actions of gentamicin (i.e., transduction channel blocking) on a healthy transduction apparatus. To test this further, we recorded responses from a hair cell (Fig. 4 *A*), and then we gently perfused the recording chamber with saline supplemented with 5 mM BAPTA, a treatment known to destroy the hair cell's tip links (Assad et al., 1991). The efficacy of the treatment in destroying the tip links was confirmed by a significant decrease in bundle stiffness from 1.15 mN m^{-1} to 0.38 mN m^{-1}, in agreement with previous work (Jaramillo and Hudspeth, 1993). This treatment completely and irreversibly destroyed the cell's ability to respond to gentamicin. Figure 4 *B*, which displays the variance of motion before and after BAPTA treatment, argues against the possibility of the variance being corrupted by artifact. This experiment was repeated in three other sacculi with identical results: a chosen cell displayed a strong response to gentamicin before BAPTA, and the response was entirely lost after treatment. Eight additional healthy-looking cells were tested after BAPTA. Although we did not record their response before BAPTA, they showed none after treatment.

A similar experiment was performed by perfusing a sacculus with saline supplemented with 100 μM gentamicin (Fig. 4 *C*). As expected, in the continued presence of a near-saturating concentration of gentamicin, this hair cell reversibly lost most of its ability to respond to iontophoretic application of gentamicin. This experiment was repeated for three other cells. In all cases, the continued presence of 100 μM gentamicin blocked the response to iontophoretic applications, although the cells' recovery following the wash was not as complete as for the cell in Fig. 4 *C*.

Time course of the variance

The variance in the attached probe's motion preceding the pulse was consistent with that expected from the combined stiffness of the probe and its coupled hair bundle. However, after the onset of bundle motion, the variance increased significantly for all cells (e.g., Fig. 3). Notice that, in subsequent figures, displacements in the negative direction are plotted as positive, allowing for easier comparison of the displacement and variance time courses. In addition, in figures in which the displacement and variance are simultaneously plotted in multiple panels (e.g., 5, 7, and 8) the variance can be easily identified as the noisier trace.

In 76 of the 96 active cells, the variance increased monotonically with a roughly exponential time course (Fig. 5). In the remaining twenty, the variance clearly reached a peak, and in sixteen of these the variance then declined to a new steady-state level (e.g., Figs. 3 and 6). In preliminary experiments, roughly similar results were observed in 47 out of 88 saccular hair cells in *Rana pipiens*. However, because responses were generally weak, we decided to switch to the more robust *R. catesbeiana* preparation (only *R. catesbeiana* data is presented here).

Many cells showed variance traces that were too noisy to be suitable for quantitative analysis. In general, this happened when responses were too small ($<$10 nm), when not enough pulses were delivered to the cell (giving rise to noisy variance traces), and when recordings were contaminated with extraneous mechanical noise. Twenty three cells were considered suitable for further quantitative analysis, 9 of which showed a clear peak in the variance, and 14 that did not.

Mathematical model and quantitative analysis

To develop a detailed model of adaptation, we would need to know the number of myosins per motor complex, the myosin's working distance, ATPase rate, the precise geometrical arrangement of the myosins comprising a motor complex, the mechanical properties of the myosin (i.e., its stiffness), the mechanical interactions between myosins, and the dependence of the myosin's working distance and ATPase rate on the load. One would also need detailed information about the regulation of the myosin's activity by Ca^{2+}, and therefore, on the regulation of intracellular Ca^{2+} concentration. Unfortunately, although we know that dozens of Myolc molecules are associated with the electron-dense insertional plaques, which are thought to anchor tip links to the stereociliary cytoskeleton, a detailed description of adaptation motor complexes is simply not available (García et al., 1998; Steyger et al., 1998). Thus, to develop a detailed stochastic model of adaptation is beyond our current capability. However, the basic characteristics of the observed displacement and variance during gentamicin application can be described by a model of adaptation in which a motor complex climbing along a stereocilium exerts a force on the hair bundle and attached probe via an elastic linkage, which is either the tip link or some other elastic element in series with it (Howard et al., 1988).

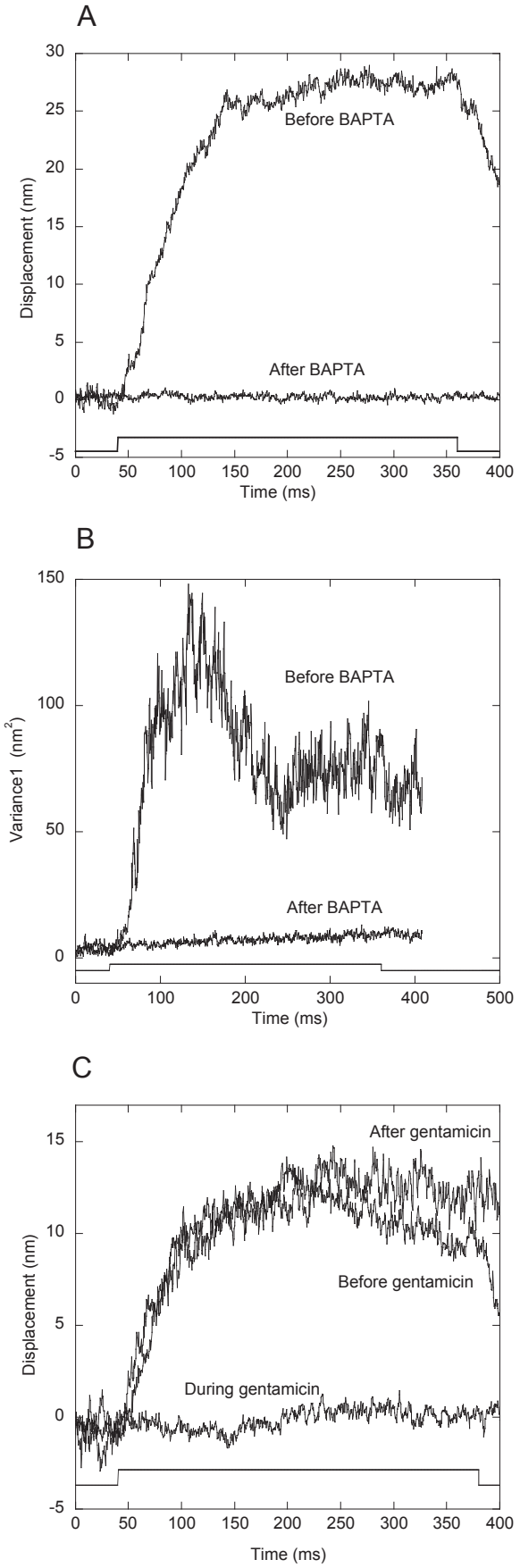

In the following equations, x refers to a projection of the displacement of the adaptation motor along the stereocilium onto the axis of mechanoelectrical sensitivity (Fig. 1). The reference point, $x = 0$, is selected such that there is no tension in the gating spring at this point. Let us assume that adaptation is characterized by two processes: an active one, due to adaptation motors *climbing* along the actin cytoskeleton, and a passive one, *slipping*, due to the tension in the gating spring. Let v_{slip} and v_{climb} represent the velocities of slipping and climbing adaptation, respectively (see Table 1 for a list of model and hair cell parameters). At rest, climbing and slipping equilibrate each other, so that $v_{climb} + v_{slip} = 0$.

We now consider adaptation after a gentamicin pulse. Notice that the model makes no assumption about the extent of blocking after a gentamicin pulse. Thus, incomplete blocking has few implications for our discussion. However, for simplicity, we assume that blocking (to whatever extent it occurs) is instantaneous. Our calculations suggest that blocking is nearly complete within a span of 10 ms (see Materials and Methods).

Slipping adaptation

Let the velocity of slipping adaptation after gentamicin be proportional to the extension of the gating spring, which is x,

$$v_{slip} = -\alpha x. \quad (1)$$

Climbing adaptation

Let us visualize climbing adaptation as consecutive steps of length h_0 and random frequency f (note, again, that h_0 refers to a projection of the displacement of the adaptation motor along the stereocilium onto the axis of mechanoelectrical sensitivity. See Fig. 1 *B*). If we assume the motor's stepping frequency to be constant, f_0, then the climbing adaptation speed would simply be $f_0 h_0$, and then we would expect both displacement and variance to follow a single exponential time course (see Derivation below). However, because the

FIGURE 4 Specificity of gentamicin action. (*A*) After the displayed responses to gentamicin (50-nA pulses) were recorded, the sacculus was perfused with recording saline supplemented with 5 mM BAPTA, which is known to destroy tip links. This treatment irreversibly destroyed the cell's ability to respond to iontophoretic gentamicin application. The stiffness of the hair bundle declined from 1.15 mN m^{-1} before BAPTA to 0.38 mN m^{-1} after treatment. (*B*) Variance corresponding to the displacement traces shown in *panel A*. (*C*) Treatment of a different hair cell with saline supplemented with 100 μM gentamicin blocked the cell's response to 25-nA iontophoretic application of the same drug. After a thorough wash, the cell recovered fully. The bundle stiffness was estimated at 1.28 mN m^{-1} before, 1.3 mN m^{-1} during, and 0.97 mN m^{-1} after bath application of gentamicin.

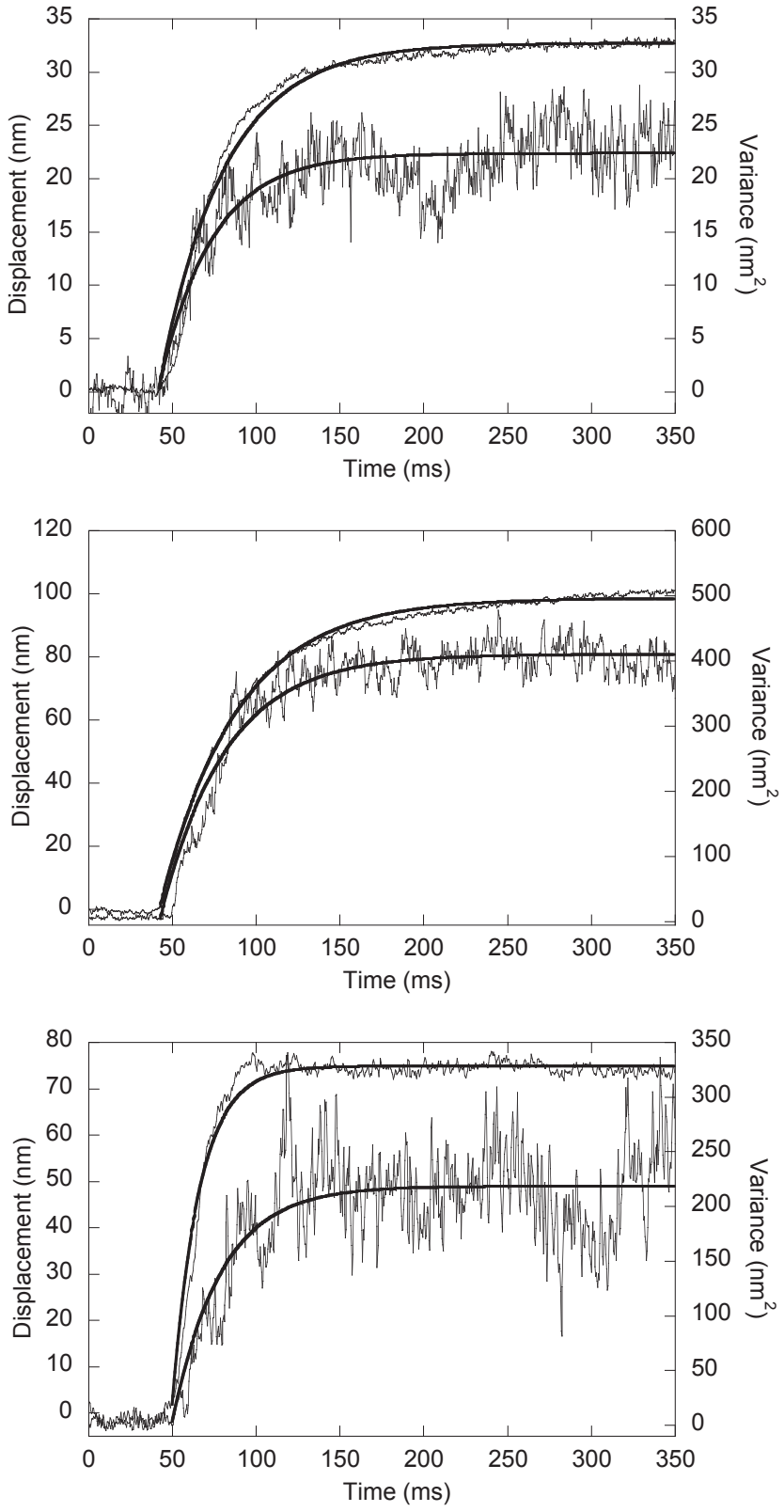

FIGURE 5 Representative examples and model fits of cells in which the variance appeared to reach a steady state without a peak. The displacement baseline (determined as the average for the 50 ms preceding the iontophoretic pulse) was subtracted. Traces were fitted to Eqs. 8 and 9. *Top*, $f_0 = 0.684$ ms^{-1}, $h_0 = 1.2$ nm; *middle*, $f_0 = 0.573$ ms^{-1}, $h_0 = 3.15$ nm; *bottom*, $f_0 = 0.871$ ms^{-1}, $h_0 = 4.82$ nm. In every panel, the variance is the noisier trace.

variance did not display a single exponential time course for a significant fraction of the cells, we decided to expand our model. We can explain both types of variance, those characterized by a single exponential time course, and those

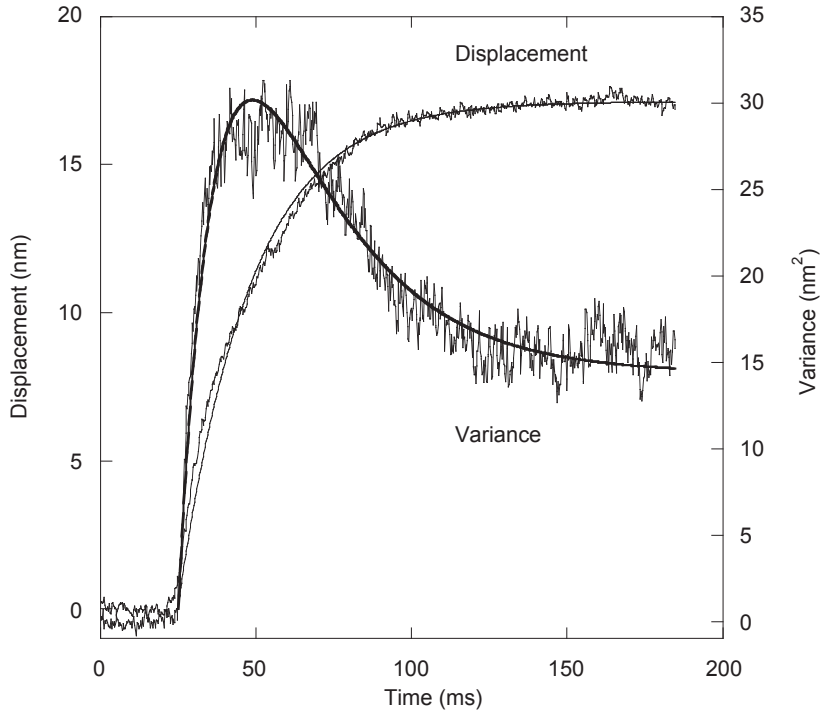

FIGURE 6 Model fit for a cell whose variance reached a well-defined peak. The displacement baseline (determined as the average for the 50 ms preceding the iontophoretic pulse) was subtracted. Displacement is fitted according to Eq. 5. The variance fit (to Eq. 6) was constrained by using the values of λ and f_0h_0 obtained from displacement. This permits us to find that, for this cell, $h_0 = 5.9$ nm, $f_0 = 0.13$ ms^{-1}, $\beta = 0.027$ nm^{-1}, and $\lambda = 0.042$ ms^{-1}.

where the variance peaks and then declines to a new steady state, by assuming that the stepping frequency can depend on the tension in the gating spring.

Then one can write

$$v_{\text{climb}} = h_0 f(1 - \beta x). \tag{2}$$

TABLE 1 Adaptation model and hair cell parameters

α	Slipping adaptation rate constant
β	Parameter that accounts for a reduction in the climbing frequency as a function of tip-link tension (see Eq. 2)
δ	Motor's step size (along y-axis)
κ_b	Stiffness of the bundle ($\sim$1 mN m^{-1})
κ_p	Stiffness of the probe ($\sim$0.75 mN m^{-1})
κ_g	Stiffness of a single tip link ($\sim$0.5 mN m^{-1})
γ	Geometrical gain, defined as the rate of change of the distance, l_t, between the tips of neighboring stereocilia with displacement, x, of the hair bundle: $\gamma = dl_t/dx$; usually this value is $\sim$0.14.
N	Number of stereocilia ($\sim$50)
φ	Force exerted by a single tip link along the stereocilia (y axis)
F_b	Net force exerted by all pivots in the bundle along x axis at the level of the probe
F_p	Force exerted by the probe along x axis
F_g	Net force exerted by all gating spring along x axis
h_0	Bundle/probe displacement resulting from motor taking a step
x	Bundle position along its axis of mechanoelectrical sensitivity. In the model equations, 1–9, the motion of the motor along the stereocilium is projected onto this axis.
y_m	Position of a motor at a stereocilium
y_m^0	(Coordinate system along the stereocilium, y axis). Same when there is no tension in the spring; depends on displacement x.
l_g	Elongation of a gating spring ($y_m - y_m^0$)

For hair cell parameters, see Howard and Hudspeth, (1988).

Then,

$$\frac{dx}{dt} = v_{\text{slip}} + v_{\text{climb}}, \tag{3}$$

hence,

$$\frac{dx}{dt} = -\alpha x + hf(1 - \beta x). \tag{4}$$

We consider the process of climbing (and slipping) as a stochastic one. This can be done by considering the frequency of climbing steps as a random parameter with an average value of f_0. Then the displacement x is a random function and Eq. 5 gives the average displacement:

$$\langle x \rangle = \frac{f_0 h_0}{\lambda}(1 - e^{-\lambda t}), \tag{5}$$

where λ describes the adaptation rate, and the variance is

$$\sigma^2 = \frac{f_0 h_0^2}{\lambda}\left[\frac{1}{2}(1 - \xi)^2 - \frac{1}{2}(1 - \xi)(1 + 3\xi)e^{-2\lambda t} + \xi^2 \lambda t e^{-2\lambda t} + 2\xi(1 - \xi)e^{-\lambda t}\right], \tag{6}$$

where

$$\lambda = \alpha + \beta f_0 h_0 \quad \text{and} \quad \xi = \frac{\beta f_0 h_0}{\lambda}. \tag{7}$$

Eq. 6 was derived by standard methods of the theory of stochastic processes (van Kampen, 1997).

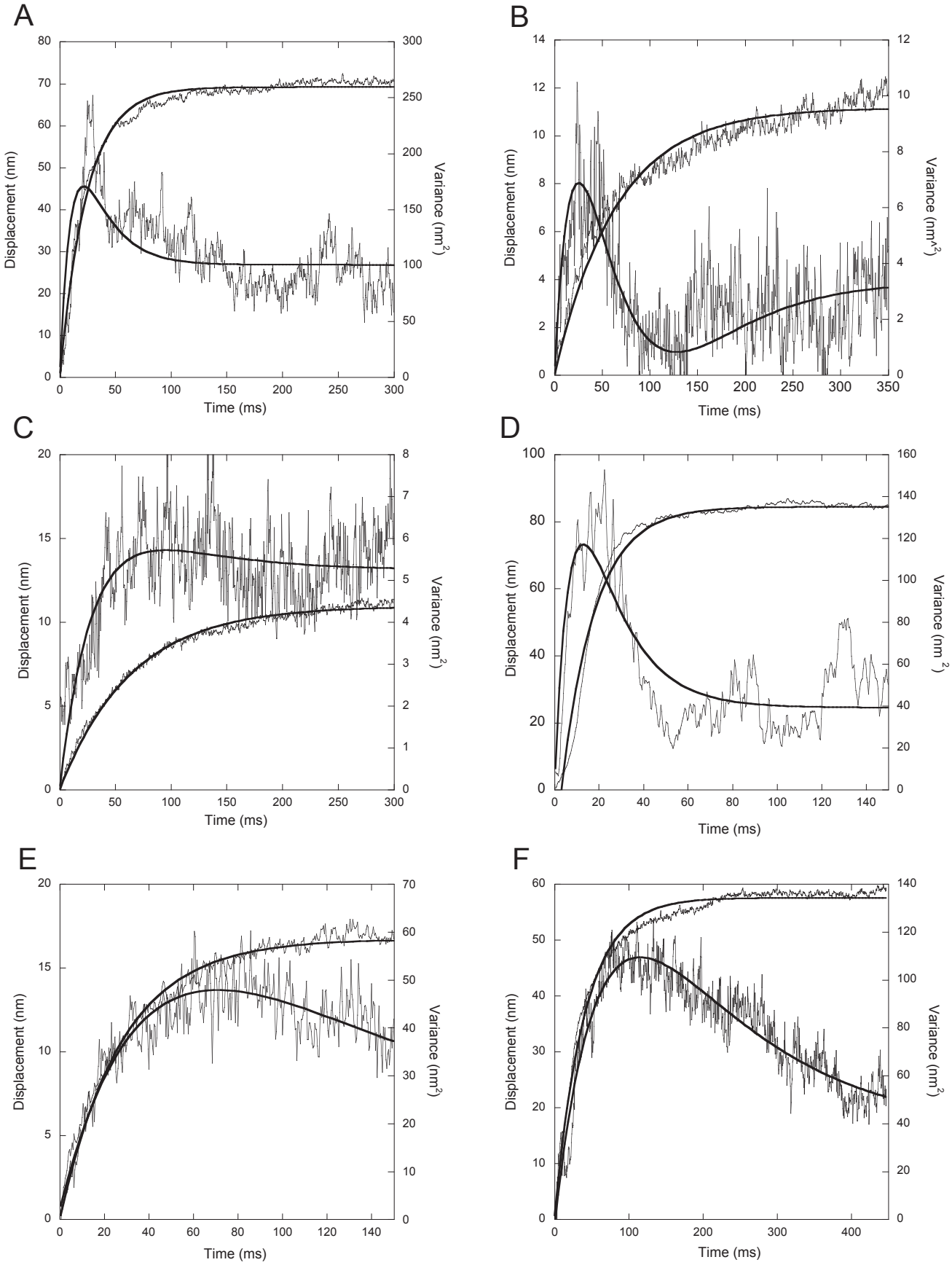
A
Displacement (nm)
Variance (nm^2)
Time (ms)
B
Displacement (nm)
Variance (nm^2)
Time (ms)
C
Displacement (nm)
Variance (nm^2)
Time (ms)
D
Displacement (nm)
Variance (nm^2)
Time (ms)
E
Displacement (nm)
Variance (nm^2)
Time (ms)
F
Displacement (nm)
Variance (nm^2)
Time (ms)

In the majority of the cells that responded to gentamicin, there was no evident decline in the variance during the pulse (Fig. 5). It is reasonable to assume that, in their case, the frequency of motor stepping was nearly independent of tension ($\beta \sim 0$). In this case, the model simplifies to

$$x = \frac{fh}{\alpha}(1 - e^{-\alpha t}) \tag{8}$$

and

$$\sigma^2 = \frac{fh^2}{2\alpha}(1 - e^{-2\alpha t}). \tag{9}$$

These cells had a mean displacement of 52 ± 30 nm (range 20–120 nm), and a mean time constant for displacement of 32 ± 30 ms (range 7–111 ms, $n = 14$). The displacement and variance traces for these cells were fitted to Eqs. 8 and 9, respectively (Fig. 5). Using these fits, the motor's step length, h_0, and stepping frequency, f_0, were estimated at 4.17 ± 2.23 nm, and 540 ± 530 s^{-1}, respectively ($n = 14$).

Although the majority of cells displayed a monotonically increasing variance, a significant fraction showed a clear peak followed by a decline to a new steady state. The proposed model provided good fits for both displacement and variance for these cells (Fig. 6). Displacement traces were fitted according to Eq. 5, yielding estimates for f_0h_0, and λ. Variance traces were fitted to Eq. 6 with two parameters (λ and h_0), and using the values of f_0h_0 and λ obtained from displacement to constrain the fits. The motor's step length, h_0, and stepping frequency, f_0, were estimated at 4.15 ± 2.17 nm, and 297 ± 240 s^{-1}, respectively ($n = 9$). Notice that the estimate for h_0 is similar to that obtained in cells whose variance did not show a clear peak, whereas f_0 is about half as large, although a *t*-test showed this difference to be not significant ($p > 0.05$).

The time course of displacement was relatively consistent from cell to cell. However, for these cells, variance was quite heterogeneous. A representative sample of these responses is shown in Fig. 7. For some cells (e.g. Fig. 7, *E* and *F*), the variance fit was poor when it was constrained to use the values of f_0h_0 and λ obtained from the displacement trace. The fits shown for these cells (Fig. 7, *bottom*) were obtained according to Eq. 6, using four free parameters (f_0, h_0, λ, and ξ). An increased number of free parameters obviously allows for better fits, but at the expense of an increase in the variability of the parameter estimates. Fits obtained for these cells were not included in our average. In a few other cases (Fig. 7 *B*), the variance declined to a local minimum, and then rebounded. Such a pattern indicates that, at some point $\beta x > 1$, which can be interpreted as tension causing the motors to stall, and then causing them to reverse (Eq. 2). In at least one case (not shown), such rebound was accompanied by a partial (although small) reversal of bundle motion. Although the model formally describes these results, it seems highly unlikely that the motor could be run in reverse. Again, these fits were excluded from our averages, although the values obtained are quite comparable to those obtained for other cells (legend of Fig. 7 *B*).

Frequently, the variance during a gentamicin pulse exhibited strong oscillations (Fig. 7). These oscillations were absent or greatly reduced before the pulse, indicating that they are related to the activity of the adaptation machinery. It is not possible to say whether these oscillations are physiologically significant because their frequency (~40 Hz) is similar to that of the main source of uncontrolled mechanical vibrations in the probe (Fig. 2). Thus, variance oscillations, even if they reflect the activity of adaptation motors, could be induced by a periodic oscillation in the glass probe. The observed variance oscillations might be explained by expanding the model to include other aspects of adaptation, (e.g., Ca^{2+} regulation in the stereocilium could lead to Ca^{2+} oscillations). An alternative source of oscillations could be oscillations in the membrane potential, and therefore in the driving force for Ca^{2+}, after channel blocking (Lewis et al., 1988). However, it is not simple to predict how factors such as these would affect displacement, or even less, variance. Note that even a simple model of adaptation produces a fairly complex expression for variance (Eq. 6). Thus, we gave variance oscillations no further consideration, although we acknowledge that the model proposed captures only the essential features of the displacement and variance time courses. Ideally, one would conduct these experiments under whole-cell clamp, which also allows for the introduction into the cell of reagents such as ADP analogs, which can block the adaptation machinery (Holt et al., 2002). However, frog epithelial cells (as opposed to dissociated cells with exposed basolateral surfaces) are difficult to patch clamp. This difficulty, in addition to the simultaneous managing of iontophoresis and stimulus probe control, poses an experimental challenge that we were not able to meet.

In general, cells clearly belonged to one of the two categories described, i.e., when subjected to several trials, cells displayed either a monotonically increasing variance

FIGURE 7 Representative examples of cells in which the variance peaked, and then declined. The displacement baseline (determined as the average for the 50 ms preceding the iontophoretic pulse) was subtracted. The traces, which, in this figure, begin at the point at which a significant departure from the baseline occurred, were preceded by a flat baseline. (*A*) $f_0 = 326\ s^{-1}$, $h_0 = 8.7$ nm, $\beta = 0.006$, $\lambda = 0.041$. (*B*) $f_0 = 420\ s^{-1}$, $h_0 = 4.11$ nm, $\beta = 0.124$, $\lambda = 0.015$. (*C*) $f_0 = 126\ s^{-1}$, $h_0 = 1.36$ nm, $\beta = 0.015$, $\lambda = 0.016$. (*D*) $f_0 = 780\ s^{-1}$, $h_0 = 6.0$ nm, $\beta = 0.007$, $\lambda = 0.056$. (*E* and *F*) were fitted with four free parameters (see Results). In every panel, the variance is the noisier trace.

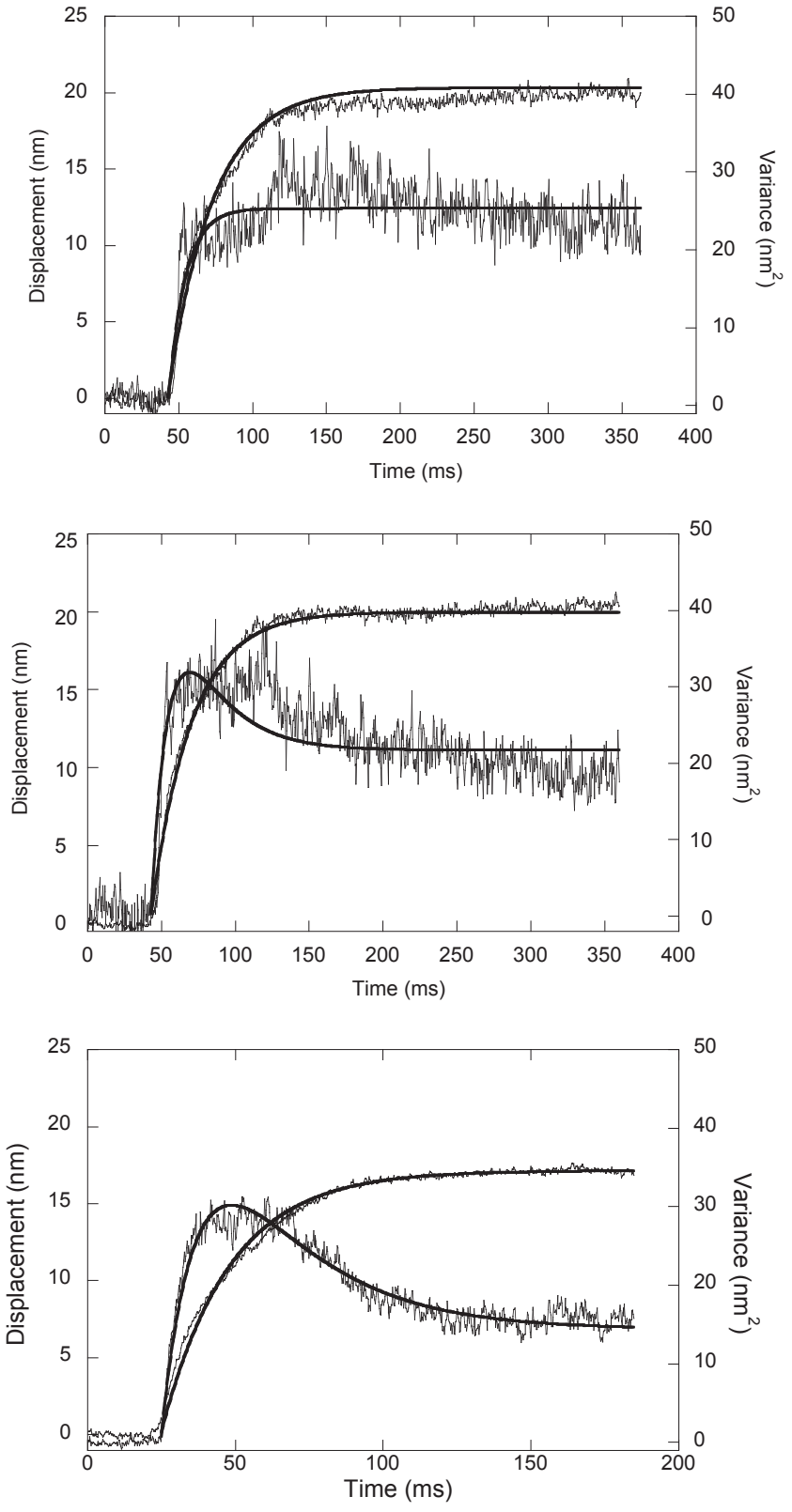

FIGURE 8 Time-dependent changes in hair bundle responses. This figure illustrates the responses of one of the three cells for which the decline in variance became more pronounced for successive stimulus runs. Every run consisted of ~50 pulses, and successive runs (from top to bottom) were started within a couple of minutes of the previous run's end. Estimates for h_0 for the three successive runs were 4.25, 5.28, and 5.85 nm respectively, whereas the estimates for f_0 were 196, 140, and 126 s^{-1} (the runs for the other two cells that showed a similar behavior were also best fitted with successively reduced estimates for f_0). In every panel, the variance is the noisier trace.

or one with a clear peak, and this behavior was maintained from trial to trial. However, in three cases, we observed a "dual" behavior (one example is shown in Fig. 8). In these three cells, the earlier runs (each consisting of several dozen

pulses) displayed a variance that showed no evident decline. However, subsequent runs obtained within a few minutes displayed a progressively more pronounced peak in the variance. These cells also showed a certain fatigue, as evidence by reduced displacements in response to the same iontophoretic pulses. For the cell shown in Fig. 8, the estimates for h_0 for the three successive runs were 4.25, 5.28, and 5.85 nm, respectively, whereas the estimates for f_0 were 196, 140, and 126 s^{-1}. The runs for the other two cells that showed a similar behavior were also best fitted with successively reduced estimates for f_0, but, notice that, for this cell, the step-size estimates change in the opposite direction. The variability of these estimates is considerably lower than for the entire cell population, suggesting that the variability in our overall estimates reflects the heterogeneity of the cell population, rather than the uncertainty of individual run estimates.

DISCUSSION

Motor activity

Consistent with previous observations, after the application of gentamicin, the hair bundle moves to a new steady-state position with an exponential time course (Jaramillo and Hudspeth, 1993). At this new position, the higher activity of the motor is balanced by an increase in slippage (see Eq. 4). Similar bundle movements are elicited when resting Ca^{2+} influx is prevented by depolarizing the cell to a potential near E_{Ca} (Assad et al., 1989). At the steady state, the motor activity settles to a value intermediate between that preceding the gentamicin pulse and that immediately following it.

Fast adaptation in *Rana* hair cells occurs when transduction channels open, allowing Ca^{2+} to permeate through the transduction channel and to promote a fast transition to the closed state (Howard and Hudspeth, 1987b). This form of adaptation is greatly diminished at the low Ca^{2+} concentration used for our recordings (Jaramillo et al., 1990). Furthermore, the blocking of the channels by gentamicin prevents Ca^{2+} entry, preventing any fast adaptation from taking place. So, fast adaptation can be ignored here.

The model we present here explains the time course of bundle motion. Furthermore, the model also predicts a gradual decline in motor activity as tension in the gating spring gradually increases (Eq. 2). Such a decrease cannot be inferred from the bundle's time course of motion (the model predicts an exponential time course regardless of β), but only from the time-dependent decrease in the bundle's variance. Cells in which both displacement and variance increase monotonically can be simply explained by the motors' independence from their load (i.e., $\beta \sim 0$).

We attribute the variance's decline to a reduction in the motor's stepping frequency, f, and therefore, ultimately to the ATPase rate of the myosins. This interpretation is consistent with the Fenn effect in muscle, which is thought to reflect a decrease in myosin's ATPase rate with an increasing load (Howard, 2001). A similar effect has been observed for kinesin, whose ATPase rate declines as the load increases, without an observable decline in the motor's working distance (Crevel et al., 1999; Meyhöfer and Howard, 1995; Visscher and Schnitzer, 1999).

How would the model change if we assumed a decrease in the motor's working distance with increasing load? Although there is no precedent for such a reduction in working distance with load, the solution of the model would be identical because the action of $1 - \beta x$ on Eq. 2 can be alternatively viewed as acting on the working distance, h.

Alternative sources of variance

Flicker block

Gentamicin leads to the activation of the adaptation machinery by acting as an open channel blocker (Denk et al., 1992; Kroese et al., 1989) to prevent the entry of Ca^{2+} through transduction channels open at rest. Thus, rapid "flicker block" could, in principle, create rapid fluctuations in the concentration of intracellular Ca^{2+}, which in turn could result in fluctuations in the activity of adaptation motors. Several arguments suggest that this is an unlikely possibility: at rest, and in the absence of blockers, transduction channels rapidly fluctuate between their open and closed states, maintaining an average open channel probability of $\sim$0.15. Yet, these rapid fluctuations do not result in any significant increase in Brownian motion of the hair bundle, which can be accounted for by the bundle's passive mechanical properties (Denk et al., 1989; Howard and Hudspeth, 1987a). Furthermore, an analysis of bundle fluctuations in the presence of gentamicin using laser interferometry revealed no component of hair bundle variance that could be attributed to flicker block (Denk et al., 1992).

Previous observations indicate that blocking in response to iontophoretic administration of gentamicin is in equilibrium with transduction channel gating (Jaramillo and Hudspeth, 1991). This is confirmed by measurements in the presence of varying nonsaturating concentrations of gentamicin, where one observes varying peak transduction currents (unpublished observations). These observations indicate that blocking is in equilibrium with the opening of transduction channels (i.e., the binding rate is much faster than changes in the binding site exposure that results from gating), which, in typical experiments, is limited by the bandwidth of hair bundle stimulation (at least 1 kHz). Compare this with the low characteristic frequency of slow adaptation ($\sim$10 Hz), or with the catalytic rate of Myo1c at saturating ATP concentrations (0.75 s^{-1}) (Gillespie et al., 1999). Therefore, the simplest explanation for the lack of a "flicker block" effect is that blocking by gentamicin is characterized by frequencies that exceed the time responsiveness of the adaptation machinery.

Transduction channel gating effects

When a closed transduction channel opens in the presence of gentamicin, blocking causes it to keep the channel gate open, because the channel cannot close while blocked. This shift in the position of the gate causes the appearance of a channel "gating force," which acts on the bundle (Denk et al., 1992; Jaramillo and Hudspeth, 1993). Therefore, fluctuations in the position of multiple gates, due to the random binding and unbinding of gentamicin, cause a fluctuating force in the hair bundle that can be measured experimentally (Denk et al., 1992). Several lines of reasoning strongly suggest that the contribution of these forces to our results is negligible: First, the cumulative impact of gating forces, even if synchronously exerted when the channels are blocked en masse, is minor, that is, peak gating forces are several-fold smaller than those exerted by adaptation motors (Denk et al., 1992; Jaramillo and Hudspeth, 1993). Second, in the presence of concentrations of gentamicin sufficient to abolish the gating compliance (the change in bundle stiffness associated with channel gating), these fluctuations are actually suppressed, causing a reduction in hair bundle fluctuations to levels below those observed in the absence of the drug (Denk et al., 1992). As discussed in Materials and Methods, we estimate that, by the end of the iontophoretic pulse, the concentration of gentamicin at the bundle should be near 400 μM, much larger than 8 μM, the estimated Kd for drug binding to the hair bundle (Kroese et al., 1989). So, one would expect bundle fluctuations at the end of the pulse to be below those observed before the pulse's onset! However, we observed no such disappearance in bundle fluctuations with time.

Third, to discount the significance of these gating effects, it is not necessary to make assumptions about the efficacy of channel blocking. Consider a typical saccular bundle with a stiffness of 1.35 mN m^{-1} resulting from the summed contributions of passive elastic elements (0.81 mN m^{-1}) and of the "gating springs" (0.54 mN m^{-1}) (Howard and Hudspeth, 1988), attached to a typical glass probe with a stiffness of 0.75 mN m^{-1}. An approximation of the variance in the position of this ensemble follows from the equipartition theorem: given the stiffness of the hair bundle and attached probe, K_{bp}, the variance of motion, σx^2, can be estimated as $\sigma x^2 = kT/k_{bp}$, where k and T have their usual thermodynamic meaning, yielding an estimate 1.9 nm^2, which is in good agreement with our observations. How much could fluctuations increase if, per chance, we had the nonsaturating gentamicin concentration that maximizes the contribution of gate fluctuations? To estimate this, we can repeat these calculations, but now omitting the contribution of the gating springs to the bundle's stiffness (0.54 mN m^{-1}). In other words, let us imagine that we have the full weight of the gating compliance working against us (Howard and Hudspeth, 1988). In this case, the variance would increase to 2.6 nm^2, an overall increase of 37%. Contrast this with the increases in variance (at least ten-fold) described in the Results.

Variability in the bundle's time course of movement between trials

The model of adaptation that we have presented here predicts hair bundle fluctuations that occur during a single trial. However, the model also implies that the time course of successive trials should also be different. Thus, variability in the time course of bundle movement between trials is expected. Furthermore, it is unlikely that random differences in the time course of motion could account for the peak in variance observed in numerous cells, because, generally, cells displayed a consistent variance type from trial to trial (see Results, and Dual Behavior below).

Time course variability is superimposed on the Brownian motion due to the passive mechanical properties of the bundle and probe. In general, the step size of molecular motors is well above this Brownian motion. Thus, we expected that motor activation would cause the increase in the variance of motion that we have reported here. However, our findings do not prove that the only source of variance following motor activation is the motor's intrinsic noise (as assumed in our model). Different sources of variance such as variability in the concentration of gentamicin near the bundle, membrane potential, Ca^{2+} buffering, etc., can conceivably be responsible for a significant part of the variance.

During the past decade, a strong yet circumstantial case for the involvement of myosin in slow adaptation has been built (Gillespie and Corey, 1997; Gillespie and Walker, 2001). Recently, a direct link between Myo1c and adaptation has been established by experiments that studied adaptation in hair cells expressing a mutated form of Myo1c that conferred sensitivity to N^6-modified ADP analogs (Holt et al., 2002). Thus, an understating of the action of adaptation motors in vestibular hair cells must take into account the stochastic properties of the individual myosin molecules that almost certainly comprise it. If adaptation motors are coupled to tip links, then it is inescapable that the random fluctuations that Myo1c molecules undergo must result in changes in tension in the tip link, and therefore, must result in increased bundle fluctuations. Even if the details of our model are incorrect, it seems plausible that the observed increases in variance reported here have their origin in the action of myosins.

Dual behavior

Estimates for f_0 for cells whose variance did not show a clear peak were about twice as large as for those who did. Although the difference is not statistically significant (as

determined by an unpaired *t*-test), the same trend was exhibited by individual cells that displayed both behaviors. In these cases, the cells started with variance timecourses that reached a steady state (without an obvious decline), but gradually shifted to variance timecourses showing a clear peak. It is possible that this shift reflects a gradual fatigue in the adaptation machinery, a fatigue that would be reflected in reduced motor stepping frequencies. It is possible that those cells showing a clear variance peak represent a subpopulation of cells with relatively depleted ATP levels, which are unable to sustain motility as effectively as the rest. Thus, the sensitivity of the motor to tension, β, might depend on the intracellular ATP concentration. An alternative explanation is that the forces generated in response to repeated stimulation disrupt the adaptation machinery. In this regard, it is worth noting that gentamicin can permeate through the transduction channel (although the extent is unknown, C. J. Kros, U. of Sussex, personal communication), perhaps damaging the adaptation machinery.

Model parameters

Hair bundle displacement and variance are reasonably well explained by the stochastic operation of a single motor. The notion of a lumped motor can be extended to N motors operating independently. In that case, the contributions of a motor to the bundle's variance could add linearly to that of its independent neighbors. This view describes more accurately the situation in the hair bundle in which numerous motors, each coupled to an individual tip link (about 50 in *R. catesbeiana* saccular hair cells), are able to operate largely independently from each other. Although all motors experience similar loads, which depend on the bundle position, the operation of a particular motor has little effect on the state of its neighbors. If we assume our cells to have ~25 intact tip links (and the same number of motors), a reasonable number following dissection and digestion (Assad et al., 1991), then a linear contribution by them would imply a stepping frequency per motor complex of $\sim 540/25\ s^{-1}$, that is $\sim 22\ s^{-1}$. A motor complex's stepping frequency could be equated with its total ATPase rate, due to the combined ATPase activity of its constituent myosins. Myo1c's ATPase rate in vitro is $\sim 0.75\ s^{-1}$ (Gillespie et al., 1999), placing it in the low extreme for myosin (Howard, 2001). Nonetheless, fewer than 29 Myo1c molecules could account for the observed stepping frequency of a motor complex. Because it is thought that each motor is composed of 100 or so myosins (García et al., 1998; Steyger et al., 1998), the data presented here suggest that only a relatively small fraction of the myosins are engaged at any one time, consistent with the view of myosin as a low duty ratio motor (Howard, 2001).

The step size for the motor, h_0, was estimated at 4.2 nm. This is an apparent (i.e., projected) motion registered by the probe along the axis of mechanical sensitivity (see Fig. 1 *B*). The relationship between the motion of the motor complex, δ, and the apparent motion measured with the probe, h_0, is (see Appendix)

$$\delta = \left(\gamma + \frac{\kappa_b + \kappa_p}{N\gamma k_g}\right) h_0. \tag{10}$$

Here γ (~ 0.14) is the lever ratio of bundle displacement to change in tip link extension, also known as the *geometrical gain*, κ_p is the stiffness of the glass probe, κ_g is the stiffness of a single tip link ($\sim 0.5\ mN\ m^{-1}$), and N is the number of stereocilia (Howard et al., 1988). With the assumed value of 25 for N our estimate of δ would be 3.6 ± 2.17 nm ($n = 9$). Thus, the apparent working distance of a single motor is comparable to that of myosin (~5 nm) (Howard, 2001). Smaller values (down to ~1.4 nm) would be obtained if a larger number of intact tip links (up to 50) is assumed. A working distance for adaptation motors somewhat below that observed for individual myosins is reasonable because a myosin's step does not fully translate into motion of the entire motor, because of the stiffness contributed by other myosins that are attached while an active one undergoes its power stroke.

The combination of step size (3.6 nm) and stepping frequency ($22\ s^{-1}$) leads to an estimate for the climbing rate of the motor along the stereocilium of $79\ nm\ s^{-1}$, which is considerably lower than the 1000–2000 $nm\ s^{-1}$ obtained from the time course of adaptation of mechano-electrical transduction currents (Hacohen et al., 1989). However, these larger values are maximum estimates for the rate at which the unloaded motor might climb, whereas, in our case, the motor experiences a significant load due to the resting tension in the tip links. This tension, which depends on the extracellular concentration of Ca^{2+}, is considerable: in the presence of 100 μM $CaCl_2$ the probability of transduction channels being open is ~0.5 (Hacohen et al., 1989). Our climbing rate can also be compared with the rates at which Myo1c can support actin motility in vivo. Our estimate is intermediate between the rates obtained for rat Myo1c (33 $nm\ s^{-1}$, Gillespie et al., 1999) and bovine Myo1c (300–500 $nm\ s^{-1}$, Zhu et al., 1996).

Fluctuations in the position of adaptation motors have an effect on the state of transduction channels. How does noise in the adaptation machinery affect the quality of mechano-electrical transduction? Experiments on isolated hair cells indicate that, for very small signals, Brownian motion of the hair bundle enhances the signal-to-noise ratio of transduction (Jaramillo and Wiesenfeld, 1998). Whether a similar effect is observed as a consequence of adaptation motor fluctuations remains to be determined.

APPENDIX: DERIVATION OF EQUATION 10

Mechanical relationships in the system are expressed by the following equations (see Table 1 for parameter definitions):

$$d\varphi = -\kappa_g dl_g = -\kappa_g dy_m + \kappa_g dy_m^0, \quad \text{(A1)}$$

$$dy_m^0 = -\gamma dx, \quad \text{(A2)}$$

$$dF_g = \gamma N d\varphi = -\gamma N \kappa_g dy_m - \gamma^2 N \kappa_g dx, \quad \text{(A3)}$$

$$dF_b = -\kappa_b dx, \quad \text{(A4)}$$

$$dF_p = -\kappa_p dx, \quad \text{(A5)}$$

$$d(F_g + F_b + F_p) = 0, \quad \text{(A6)}$$

$$-\gamma N \kappa_g dy_m - \gamma^2 N \kappa_g dx - \kappa_b dx - \kappa_p dx = 0. \quad \text{(A7)}$$

Let us suppose that $dy_m = \delta$, and $dx = h_0$, then we obtain Eq. 10,

$$\delta = -\left(\gamma + \frac{\kappa_b + \kappa_p}{N\gamma k_g}\right) h_0. \quad \text{(A8)}$$

REFERENCES

Assad, J. A., N. Hacohen, and D. P. Corey. 1989. Voltage dependence of adaptation and active bundle movement in bullfrog saccular hair cells. *Proc. Natl. Acad. Sci. U. S. A.* 86:2918–2922.

Assad, J. A., M. G. Sheperd, and D. P. Corey. 1991. Tip-link integrity and mechanical transduction in vertebrate hair cells. *Neuron.* 7:985–994.

Berg, H. C. 1983. Random Walks in Biology. Princeton University Press, Princeton, NJ. 22–23.

Crevel, I. N., M. Carter, M. Schliwa, and R. Cross. 1999. Coupled chemical and mechanical reaction steps in a processive Neurospora kinesin. *EMBO J.*18:5863–5872.

Denk, W., R. M. Keolian, and W. W. Webb. 1992. Mechanical response of frog saccular hair bundles to the aminoglycoside block of mechanoelectrical transduction. *J. Neurophysiol.* 68:927–932.

Denk, W., W. W. Webb, and A. J. Hudspeth. 1989. Mechanical properties of sensory hair bundles are reflected in their Brownian motion measured with a laser differential interferometer. *Proc. Natl. Acad. Sci. U. S. A.* 86:5371–5375.

Eatock, R. A. 2000. Adaptation in hair cells. *Annu. Rev. Neurosci.* 23: 285–314.

García, J. A., A. G. Yee, P. G. Gillespie, and D. P. Corey. 1998. Localization of myosin-Iβ near both ends of tip links in frog saccular hair cells. *J. Neurosci.* 18:8637–8647.

Gillespie, P. G., and D. P. Corey. 1997. Myosin and adaptation by hair cells. *Neuron.* 19:955–958.

Gillespie, P. G., S. K. H. Gillespie, J. A. Mercer, and K. Shah. 1999. Engineering of the myosin-Iβ nucleotide-binding pocket to create selective sensitivity to N^6-modified ADP analogs. *J. Biol. Chem.* 274: 31373–31381.

Gillespie, P. G., and R. G. Walker. 2001. Molecular basis of mechanosensory transduction. *Nature.* 413:194–202.

Hacohen, N., J. A. Assad, W. J. Smith, and D. P. Corey. 1989. Regulation of tension on hair–cell transduction channels: displacement and calcium dependence. *J. Neurosci.* 9:3988–3997.

Holt, J. R., and D. P. Corey. 2000. Two mechanisms for transducer adaptation in vertebrate hair cells. *Proc. Natl. Acad. Sci. U. S. A.* 97:11730–11735.

Holt, J. R., K. H. Gillespie, D. W. Provance, K. Shah, K. M. Shokat, D. P. Corey, J. A. Mercer, and P. G. Gillespie. 2002. A chemical-genetic strategy implicates myosin-1c in adaptation by hair cells. *Cell.* 108: 371–381.

Howard, J. 2001. Mechanics of Motor Proteins and the Cytoskeleton. Sinauer, Sunderland, MA. 245–262.

Howard, J., and A. J. Hudspeth. 1987a. Brownian motion of hair bundles from the frog's inner ear. *Biophys. J.* 51:203a.

Howard, J., and A. J. Hudspeth. 1987b. Mechanical relaxation of the hair bundle mediates adaptation in mechanoelectrical transduction by the bullfrog's saccular hair cell. *Proc. Natl. Acad. Sci. U. S. A.* 84: 3064–3068.

Howard, J., and A. J. Hudspeth. 1988. Gating compliance associated with gating of mechanoelectrical transduction channels in the bullfrog's saccular hair cell. *Neuron.* 1:189–199.

Howard, J., W. M. Roberts, and A. J. Hudspeth. 1988. Mechanoelectrical transduction by hair cells. *Annu. Rev. Biophys. Biophys. Chem.* 17: 99–124.

Jaramillo, F., J. Howard, and A. J. Hudspeth. 1990. Calcium ions promote rapid mechanically evoked movements of hair bundles. *In* The Mechanics and Biophysics of Hearing. P. Dallos, C. D. Geisler, J. J. Matthews, M. A. Ruggero, and C. R.Steele, editors. Springer, Berlin. 26–33.

Jaramillo, F., and A. J. Hudspeth. 1991. Localization of the hair cell's transduction channels to the hair bundle's tip by iontophoretic application of channel blockers. *Neuron.* 7:409–420.

Jaramillo, F., and A. J. Hudspeth. 1993. Displacement-clamp measurement of forces exerted by gating springs in the hair bundle. *Proc. Natl. Acad. Sci. U. S. A.* 90:1330–1334.

Jaramillo, F., and K. Wiesenfeld. 1998. Mechanoelectrical transduction assisted by Brownian motion: a role for noise in the auditory system. *Nature Neurosci.* 1:384–388.

Kroese, A. B. A., A. Das, and A. J. Hudspeth. 1989. Blockage of the transduction channels of hair cells in the bullfrog's sacculus by aminoglycoside antibiotics. *Hear. Res.* 37:203–218.

Kros, C. J., W. Marcotti, S. M. van Netten, T. J. Self, R. T. Libby, S. D. M. Brown, G. P. Richardson, and K. P. Steel. 2002. Reduced climbing and increased slipping adaptation in cochlear hair cells of mice with Myo7a mutations. *Nature Neurosci.* 5:41–47.

Lewis, R. S., and A. J. Hudspeth. 1988. A model for electrical resonance and frequency tuning in saccular hair cells of the bull-frog, *Rana catesbeiana*. *J. Physiol. (Lond.).* 400:275–297.

Meyhöfer, E., and J. Howard. 1995. The force generated by a single kinesin molecule against an elastic load. *Proc. Natl. Acad. Sci. U. S. A.* 92: 574–578.

Ricci, A. J., Y.-C. Wu, and R. Fettiplace. 1998. The endogenous calcium buffer and the time course of transducer adaptation in auditory hair cells. *J. Neurosci.* 18:8261–8277.

Steyger, P. S., P. G. Gillespie, and R. A. Baird. 1998. Myosin-Iβ is located at tip link anchors in vestibular hair bundles. *J. Neurosci.* 18: 4603–4615.

van Kampen, N. G. 1997. Stochastic Processes in Physics and Chemistry. Elsevier, Amsterdam.

Visscher, K., and M. J. Schnitzer. 1999. Single kinesin molecules studied with a molecular force clamp. *Nature.* 400:184–189.

Wu, Y.-C., A. J. Ricci, and R. Fettiplace. 1999. Two components of transducer adaptation in auditory hair cells. *J. Neurophysiol.* 82: 2171–2181.

Zhu, T., M. Sata, and M. Ikebe. 1996. Functional expression of mammalian myosin 1β: analysis of its motor activity. *Biochemistry.* 35:513–522.